Crystal structure of *Escherichia coli* lytic transglycosylase Slt35 reveals a lysozyme-like catalytic domain with an EF-hand

Erik J van Asselt[1], Arnoud J Dijkstra[2], Kor H Kalk[1], Bela Takacs[2], Wolfgang Keck[2] and Bauke W Dijkstra[1]*

Background: Lytic transglycosylases are bacterial muramidases that catalyse the cleavage of the β-1,4-glycosidic bond between *N*-acetylmuramic acid (MurNAc) and *N*-acetylglucosamine (GlcNAc) in peptidoglycan with concomitant formation of a 1,6-anhydrobond in the MurNAc residue. These muramidases play an important role in the metabolism of the bacterial cell wall and might therefore be potential targets for the rational design of antibacterial drugs. One of the lytic transglycosylases is Slt35, a naturally occurring soluble fragment of the outer membrane bound lytic transglycosylase B (MltB) from *Escherichia coli*.

Results: The crystal structure of Slt35 has been determined at 1.7 Å resolution. The structure reveals an ellipsoid molecule with three domains called the alpha, beta and core domains. The core domain is sandwiched between the alpha and beta domains. Its fold resembles that of lysozyme, but it contains a single metal ion binding site in a helix–loop–helix module that is surprisingly similar to the eukaryotic EF-hand calcium-binding fold. Interestingly, the Slt35 EF-hand loop consists of 15 residues instead of the usual 12 residues. The only other prokaryotic proteins with an EF-hand motif identified so far are the D-galactose-binding proteins. Residues from the alpha and core domains form a deep groove where the substrate fragment GlcNAc can be bound.

Conclusions: The three-domain structure of Slt35 is completely different from the Slt70 structure, the only other lytic transglycosylase of known structure. Nevertheless, the core domain of Slt35 closely resembles the fold of the catalytic domain of Slt70, despite the absence of any obvious sequence similarity. Residue Glu162 of Slt35 is in an equivalent position to Glu478, the catalytic acid/base of Slt70. GlcNAc binds close to Glu162 in the deep groove. Moreover, mutation of Glu162 into a glutamine residue yielded a completely inactive enzyme. These observations indicate the location of the active site and strongly support a catalytic role for Glu162.

Addresses: [1]BIOSON Research Institute and Laboratory of Biophysical Chemistry, Groningen University, Nijenborgh 4, 9747 AG Groningen, The Netherlands and [2]F Hoffmann-LaRoche Ltd., Pharma Research Department, CH-4002 Basel, Switzerland.

*Corresponding author.
E-mail: bauke@chem.rug.nl

Key words: EF-hand, *Escherichia coli*, lysozyme, lytic transglycosylase, peptidoglycan

Received: 13 May 1999
Revisions requested: 10 June 1999
Revisions received: 8 July 1999
Accepted: 12 July 1999

Published: 14 September 1999

Structure October 1999, 7:1167–1180
http://biomednet.com/elecref/0969212600701167

0969-2126/99/$ – see front matter

Introduction

The shape and strength of the bacterial cell is largely determined by its cell wall [1]. The bacterial cell wall is made up of peptidoglycan, which, as a single molecule, surrounds the entire cell and protects the bacterium from the high internal osmotic pressure. Peptidoglycan consists of oligomeric glycan strands of alternating *N*-acetylglucosamine (GlcNAc) and *N*-acetylmuramic acid (MurNAc) residues cross-linked by short oligopeptide chains of alternating L-amino and D-amino acids. To keep the cell wall intact during cell growth and division, a large number of peptidoglycan-metabolising enzymes works closely together to prevent rupture of the cell wall and cell lysis [2]. Given that peptidoglycan is essential, unique for prokaryotes and easily accessible, the peptidoglycan-metabolising enzymes constitute effective targets for antibacterial compounds. For example, penicillin and related β-lactam antibiotics inhibit the enzymes that are responsible for the making and breaking of the peptide cross-linkages [3]. Unfortunately, the widespread use of antibiotics over the years has enhanced the development of resistance in many bacteria. An intensive search for new antibacterial agents has therefore been initiated to overcome the problem of resistance [4]. Suitable targets for such new drugs could be β-lactam insensitive peptidoglycan-metabolising enzymes, such as the lytic transglycosylases.

Lytic transglycosylases catalyse the cleavage of the β-1,4-glycosidic bond between MurNAc and GlcNAc residues in peptidoglycan with concomitant formation of a 1,6-anhydrobond between the O6 and C1 atoms in the MurNAc residue [5]. They are believed to function as space makers to allow the insertion of new peptidoglycan material into the cell wall during growth [6]. Moreover,

they are involved in making pores in the peptidoglycan layer to allow transport of DNA and proteins across the cell wall [7], and they have been proposed to act as cell wall zippers during cell division [8]. Because lytic transglycosylases are able to completely degrade peptidoglycan to 1,6-anhydromuropeptides *in vitro*, their activity *in vivo* has to be strictly controlled [8]. The regulation of their activity is not understood in detail. It has been suggested that transglycosylases closely cooperate with peptidoglycan-synthesising enzymes [9] or may be bound to them acting together as peptidoglycan-metabolising complexes [10,11].

The importance of lytic transglycosylases for the cell wall metabolism of *Escherichia coli* is indicated by the identification of one soluble (Slt70 [5]) and five membrane-bound lytic transglycosylases (MltA–D and EmtA [12–19]). They differ in size, sequence, activity, specificity and location. Homologous genes have been identified in many Gram-negative and Gram-positive bacteria [7,20,21]. Structural research on lytic transglycosylases has resulted so far in the crystal structures of the 70 kDa soluble lytic transglycosylase Slt70 [22] and its complex with the inhibitor bulgecin A [23], a naturally occurring glycopeptide produced by *Pseudomonas acidophila* and *Pseudomonas mesoacidophila*. Bulgecin is a specific inhibitor of the lytic transglycosylases Slt70 [24], MltC and MltD [18], but not of MltA or MltB.

MltB is of special interest because both a membrane-bound form and a soluble form have been identified in *E. coli* [14–16]. The membrane-bound enzyme is a 40 kDa lytic transglycosylase of 361 amino acid residues. Its amino acid sequence does not show obvious homology to that of Slt70 [15,16]. Furthermore, it is a lipoprotein that is anchored to the outer membrane via a lipid anchor attached to Cys19. The lipid anchor probably acts as a safety measure to prevent direct degradation of the cell wall [16]. Slt35 is a naturally occurring soluble 36 kDa proteolytic fragment of MltB, formed when the first 39 amino acid residues are cleaved off [14–16]. This stable fragment has been successfully overexpressed and purified [15], and it is fully active as shown by zymogram and high pressure liquid chromatography (HPLC) analysis [15].

In this article we describe the crystal structure of Slt35. One of its three domains shows a lysozyme fold and a metal ion binding site that surprisingly resembles EF-hand calcium-binding domains. Furthermore, a soaking experiment revealed the binding of the monosaccharide GlcNAc in a deep groove close to a conserved glutamate residue, which is proposed to function as the catalytic acid/base during the cleavage and transglycosylation reaction.

Results and discussion

Structure determination and description

The crystal structure of native Slt35 has been solved by the multiple isomorphous replacement method with subsequent refinement at 1.7 Å resolution to a final crystallographic R factor of 17.8%. Tables 1 and 2 and the Materials and methods section give pertinent details on the structure determination. The final model contains 312 amino acid residues (40–98 and 109–361) with alternate

Table 1

Data collection and phasing statistics.

Data set	Native	GlcNAc	Os-I*	Pb-I*	Hg-I*	Hg-II*	Hg-III*
Data collection							
Soaking							
concentration (mM)	–	Saturated	3.0	12	3.0	2.0	3.0
time	–	18 min	4 days	24 h	6 days	8 days	2 h
Resolution range (Å)	30–1.70	25–2.45	34–3.00	34–3.44	34–2.69	34–2.70	18–2.02
No. of reflections							
total	206,582	49,117	23,113	21,880	20,201	23,732	92,150
unique	43,117	14,836	7954	5096	9063	9339	24,767
Completeness (%)	97.6	98.4	96.6	91.8	80.0	82.6	94.0
R_{merge} (%)†	5.0	10.4	5.6	7.4	3.7	4.2	3.8
R_{nat} (%)‡			9.3	6.0	6.2	7.1	6.9
Phasing statistics							
Number of sites			4	2	7	5	6
Phasing power§							
iso			1.29	0.97	1.56	1.39	0.88
ano			0.51	0.37	0.69	0.69	1.20
R_{Cullis}¶			0.578	0.657	0.552	0.608	0.657
Figure of merit (overall)#			0.604				

*Os-I, $K_2OsO_4 \cdot 2H_2O$; Pb-I, trimethyllead acetate; Hg-I, parachloromercury-phenylsulphonic acid; Hg-II, parachloromercury-benzoic acid; Hg-III, 2-chloromercury-4-nitrophenol. †$R_{merge} = \Sigma|I-\langle I\rangle|/\Sigma I$. ‡$R_{nat} = \Sigma_{hkl}|(F_P-F_{PH})|/\Sigma_{hkl}\ 0.5(F_P + F_{PH})$. §Phasing power $= \Sigma_{hkl}\ |F_H(calc)|/\Sigma_{hkl}\ ||F_{PH}| - |F_{PH}(calc)||$. ¶$R_{Cullis} = \Sigma_{hkl}\ ||F_{PH} \pm F_P| - F_H(calc)|/\Sigma_{hkl}\ |F_{PH} \pm F_P|$. #For 10,418 reflections from 24.0 to 2.70 Å.

sidechain conformations for 15 residues (Asp74, Ile81, Ser83, Lys86, Leu94, Asp139, Trp145, Glu153, Ile155, Ser193, Met202, Arg204, Phe217, Asp269 and Gln311). The sidechain of the first N-terminal residue Met40 and an internal stretch of ten residues (99–108) do not show interpretable electron density in F_o–F_c and $2F_o$–F_c omit maps and have been omitted from the model. To examine whether the crystallised protein had been cleaved, Slt35 crystals were dissolved and analysed by sodium dodecyl sulphate polyacrylamide gel electrophoresis (SDS–PAGE). No cleavage of the protein was observed (data not shown).

Slt35 is very rich in α helices, but has some short β strands as well. In total, 49% of all observed 312 amino acid residues are found in 14 α helices (H1–H14), and 10% of the amino acids are found in seven β strands (S1–S7) forming two β sheets (Figures 1,2). The remaining residues are found in β turns and γ turns, loops and two 3_{10} helices. The three-dimensional structure of Slt35 is built up of three well-defined domains named the alpha, beta and core domains, and has dimensions of approximately 35 Å × 45 Å × 75 Å.

The alpha domain

The alpha domain of Slt35 is at the bottom of the structure in the orientation shown in Figure 1 and can be considered to be built up of two subdomains. The first subdomain comprises residues 40–98 and the three α helices H1, H2 and H3. Residues 40–50 are very flexible as indicated by high mean atomic displacement parameters (49 Å^2 for the mainchain and 50 Å^2 for the sidechain atoms, compared with mean B factors of 21 Å^2 and 24 Å^2 for all mainchain and sidechain atoms, respectively). This stretch of residues is only connected to the alpha domain by hydrogen bonds between the carbonyl oxygen atom of Val47 and the Nε2 atoms of Gln76 and Gln79. In the full MltB protein it might have a different conformation or be part of the flexible linker that anchors the enzyme to the outer membrane.

The second subdomain includes residues 170–215, which form a hairpin-like structure. The hairpin sequentially consists of the short β strand S1 (residues 172–173), α helix H8 (174–183), 3_{10} helix (186–188), α helix H9 (189–205), 3_{10} helix (210–212) and short β strand S2 (residues 214–215), in which the two strands form a small antiparallel β sheet. The accessible surface area buried by the interaction of the two subdomains is substantial, 1000 Å^2. The major part of this buried interface consists of hydrophobic residues with significant contributions from alanine, leucine and phenylalanine residues.

Comparisons of various MltB sequences show that the residues in the N-terminal subdomain are not conserved, whereas the residues in the hairpin subdomain display a conservation of about 43% (Figure 2). According to the DALI server [25] the overall fold of the alpha domain does not show similarity to any other protein.

Table 2

Refinement statistics.

Data set	Native	GlcNAc
Resolution range (Å)	20.0–1.70	20.0–2.45
No. of reflections		
total	41,498	14,679
work set	37,284	13,196
test set	4214	1483
Final R factor (%)*	17.8	19.5
R_{work} factor (%)†	17.6	19.1
R_{free} factor (%)‡	20.7	25.6
Rmsd		
bond lengths (Å)§	0.008	0.006
bond angles (°)§	1.3	1.2
dihedral angles(°)§	22.2	22.1
improper angles(°)§	1.21	1.05
Non-hydrogen protein atoms	2550	2507
Residues	312	312
Alternate sidechains	15	4
Solvent molecules	426	201
Bicine molecule	1	0
Ethylene glycol molecule	1	0
Metal ion	1	1
GlcNAc molecule	0	1
Average B factor (Å^2)		
Wilson plot	19.1	19.5
mainchain	20.5	20.9
sidechains	23.5	21.6
all atoms	24.6	21.8

*Final R factor = Σ_{hkl} (| F_o(hkl, all) | – | F_c(hkl, all) |) /Σ_{hkl} | F_o(hkl, all) |. †R_{work} factor = Σ_{hkl}(| F_o(hkl, work set) | – | F_c(hkl, work set) |) /Σ_{hkl} | F_o(hkl, work set) |. ‡R_{free} factor = Σ_{hkl}(| F_o(hkl, test set) | – | F_c(hkl, test set) |) /Σ_{hkl} | F_o(hkl, test set) |. §With respect to the Engh and Huber parameters [68].

The beta domain

The beta domain is located above the core domain of Slt35 (Figure 1). It consists of residues 270–329, which form a five-stranded antiparallel β sheet (S3–S7) that is flanked by one short α helix (H12) of six residues (292–297). As with the alpha domain, the beta domain seems to have a new overall fold; no similar structures could be identified by the DALI server [25]. The buried surface area between the beta domain and the core domains is large, 820 Å^2, with only three residues (Asp318, Tyr323 and Leu329) making hydrogen bonds to the core domain. The remaining interactions are hydrophobic.

The core domain

The core domain of Slt35 is sandwiched between the alpha and beta domains. It can be considered to consist of three segments (residues 109–169, 216–269 and 330–361). The residues between the first and second segment (residues 170–215) make up the second subdomain of the alpha domain and the beta domain is inserted between segment two and three. The first segment is made up of the four α helices H4, H5, H6 and H7. Residues 111 to 114 are anchored via their backbone amide nitrogen atoms to the carboxylate group and backbone carbonyl oxygen

Figure 1

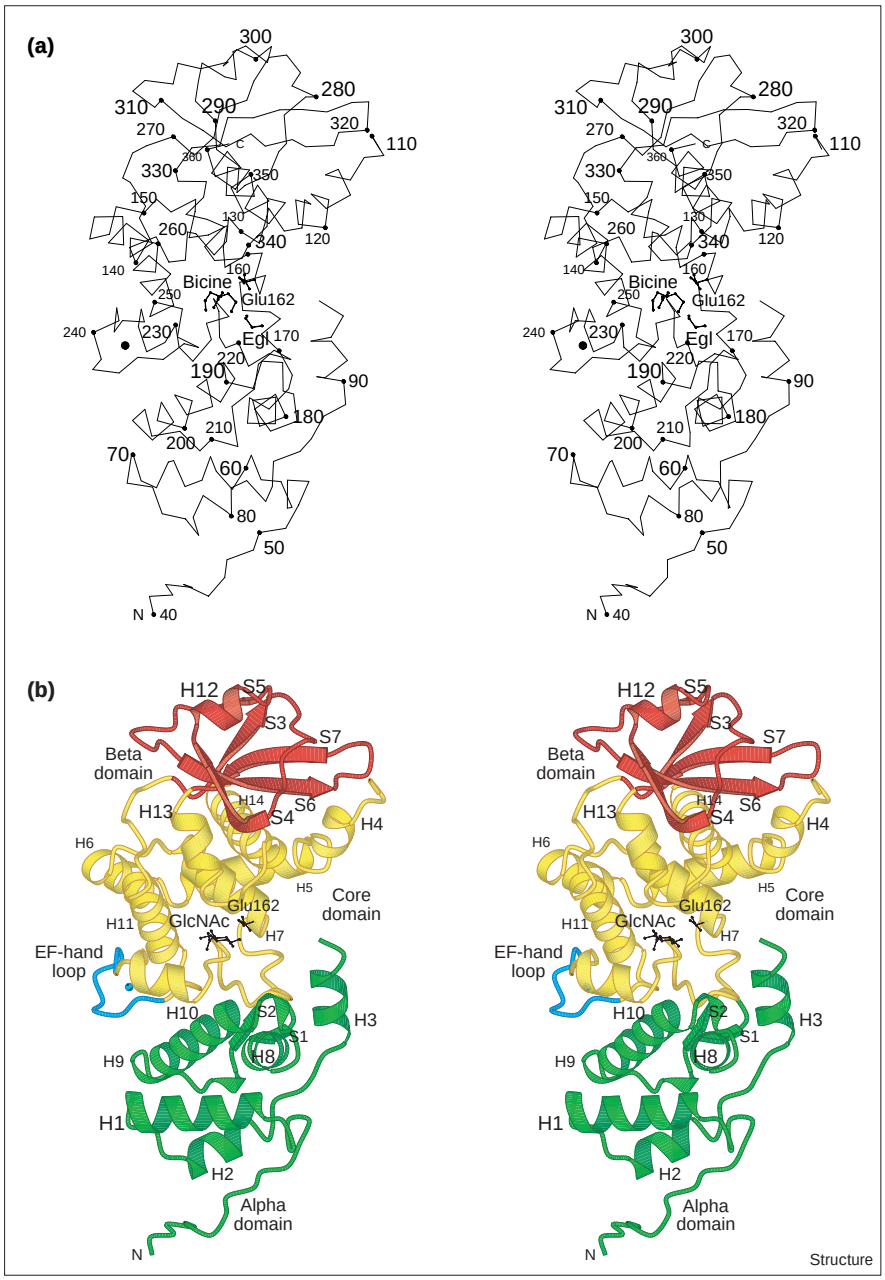

Stereoviews of Slt35. (**a**) Cα trace with bicine and ethylene glycol (Egl) molecules in the active-site groove. Every tenth amino acid residue is labelled. (**b**) Ribbon plot with GlcNAc shown in the active-site groove. The alpha domain (green) is at the bottom of the molecule, the beta domain (red) is at the top and the core domain (yellow) is in the centre. The EF-hand loop (residues 237–245) with the metal ion is depicted in blue. The secondary structure elements are labelled H1–H14 for the α helices and S1–S7 for the β strands. The proposed catalytic acid/base Glu162 and the GlcNAc molecule are indicated in ball-and-stick representation. The figure was produced with the program MOLSCRIPT [64].

Figure 2

Multiple sequence alignment, generated with CLUSTAL [65] and ALSCRIPT [66], of MltB lytic transglycosylases from *Escherichia coli*, *Salmonella typhimurium*, *Yersinia pestis* (two different MltBs labelled 1–2), *Pseudomonas aeruginosa* (four different MltBs labelled 1–4), *Bordetella pertussis*, *Neisseria gonorrhoeae*, *Neisseria meningitidis* and *Haemophilus actinomycetemcomitans*. The sequences were obtained using the BLAST server at the National Center for Biotechnology Information [67]. The residue numbering of *E. coli* MltB is displayed at the top of the alignment and the different domains and secondary structures in Slt35 are indicated at the bottom. The conserved catalytic acid/base Glu162 of Slt35 is marked with an arrow. The domain nomenclature refers to the MltB of *E. coli*. The alpha domain consists of residues 40–98 and 170–215, the beta domain of residues 270–329 and the core domain of residues 109–169, 216–269 and 330–361. Identical residues are shown as white letters on a black background; conserved residues are shaded in grey.

atom of Asp318, located at the end of β strand S6 in the beta domain. In the second segment (residues 216–269), the loop that connects α helices H10 (residues 228–234) and H11 (residues 249–262) binds a metal ion (see below). The residues in this loop and α helix H10 are the only residues in the core domain that make hydrogen bonds to

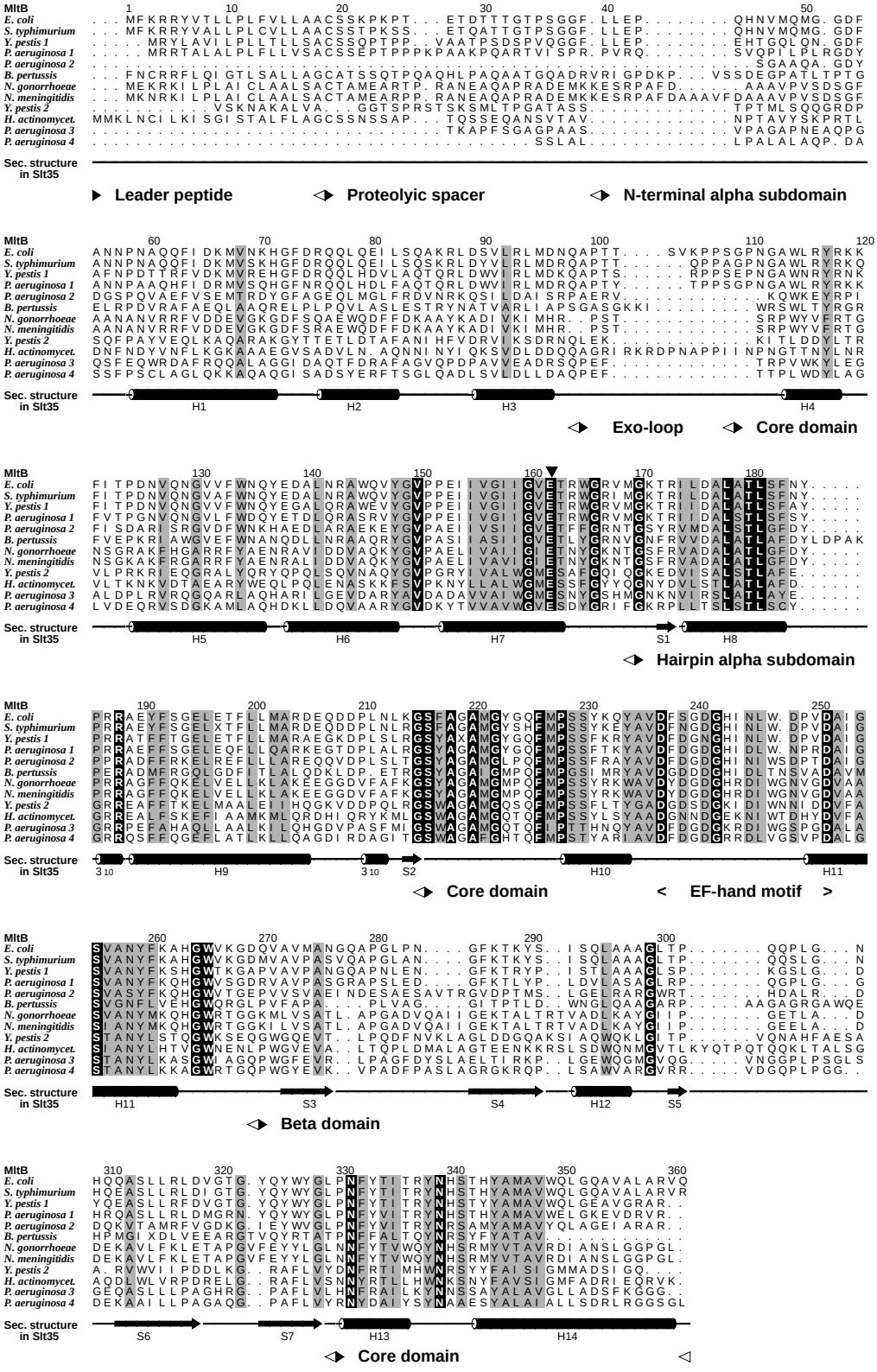

Structure

Figure 3

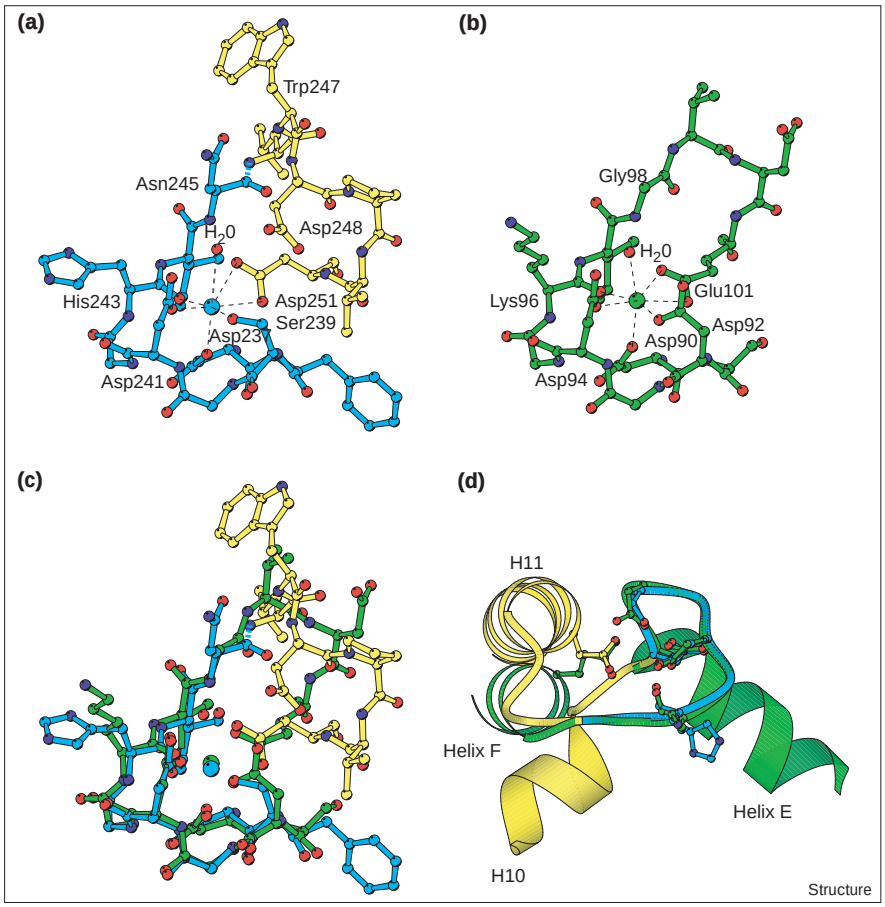

The metal ion binding sites in (a) Slt35 and (b) carp parvalbumin B (PDB entry code 5cpv). (c,d) Superposition of the metal ion binding sites in Slt35 and parvalbumin B. Part (c) shows a close-up of the binding site, (d) shows the orientation and position of the EF-hand helices in the two proteins. Residues 90–98 of parvalbumin B (green) were superimposed on residues 237–245 of Slt35 (blue) with an rmsd of 0.32 Å^2 for nine Cα atoms. Residues of Slt35 that were not used in the superposition are shown in yellow. Helices E and F (green) belong to parvalbumin and the α helices H10 and H11 (yellow) are from Slt35.

residues in the alpha domain (Pro228 and Ser229 with Glu195, and Tyr231 and Ile244 with Glu206). The buried surface between the alpha and the core domain is about 760 Å^2. The third segment contains the C-terminal residues 330–361 and the α helices H13 and H14, which provide the major interactions with the beta domain. The overall fold of the core domain resembles those of the goose-type lysozyme [26] and the catalytic domain of Slt70 [27] (see below).

A novel EF-hand motif

A metal ion is bound in the loop that connects α helices H10 and H11. Figure 3a shows the distorted octahedral coordination of the metal ion, which is ligated by six protein oxygen atoms (Oδ1 of Asp237, Oγ of Ser239, Oδ1 of Asp241, O of His243, Oδ1 and Oδ2 of Asp251) at an average distance of 2.4 Å. A water molecule is located at 3.3 Å from the metal ion. The polypeptide chain contributing these residues has a conformation that resembles the EF-hand calcium-binding domains commonly found in eukaryotic intracellular calcium-binding proteins, like calmodulin and parvalbumin [28,29]. In general, EF-hand domains consist of a 12-residue loop flanked on both sides by an α helix. In Slt35, however, the loop consists of 15 residues. The interhelical angle between α helices H10 and H11 is 75°, which is close to the range of 84–101° observed for the EF-hand domains in calmodulin [30] and carp parvalbumin B [28]. Nevertheless, as is evident from Figure 3d, α helices H10 and E are oriented differently with respect to the superimposed calcium-binding loops, and α helix H11 has been translated.

In typical EF-hand loops, the calcium ion is coordinated in a pentagonal bipyramidal configuration, whereby usually six residues contribute to the binding of the ion [28,29]. These residues are located in positions 1, 3, 5, 7, 9 and 12 of the EF-hand calcium-binding consensus sequence (Figure 4). The residue at position 7 ligates the calcium with its carbonyl oxygen atom, whereas the other residues contribute with their sidechain oxygen atoms to the metal ion coordination. The residues of Slt35 conform to this consensus motif with the exception of Asn245 at position 9 and Asp248 at position 12. The sidechain oxygen atom of Asn245 is hydrogen bonded to the amide nitrogen of Trp247 and is too far away (7.9 Å) to be a possible ligand. The ligating residue at position 9 shows great

Figure 4

Multiple sequence alignment of the EF-hand motifs of carp parvalbumin B and the MltB transglycosylases from *Escherichia coli* and *Neisseria gonorrhoea*. Residues X, Y, Z, –X and –Z coordinate the metal ion with their sidechain oxygen atoms. In some cases, a bridging water molecule is present between the sidechain and the ion. Residue –Y supplies a mainchain carbonyl oxygen atom as ligand and the carboxylate at –Z coordinates the metal ion with both oxygen atoms. X and –X define the unique axis of a pentagonal bipyramid [29]. The positions 11^a and 11^b refer to the insertion of an extra residue in the EF-hand of some MltBs in the sequence alignment of Figure 2.

Carp parvalbumin B	50	**D**	Q	**D**	K	**S**	G	**F**	I	**E**	-	-	-	-	E	D	**E**	62
Carp parvalbumin B	89	**D**	S	**D**	G	**D**	G	**K**	I	G	-	-	-	-	V	D	**E**	101
MltB from *E. coli*	237	**D**	F	**S**	G	**D**	G	**H**	I	N	L	W	-	D	P	V	**D**	251
MltB from *N. gono*	233	**D**	Y	**D**	G	**D**	G	**H**	R	D	I	W	G	N	V	R	**D**	248
Coordination		**X**		**Y**		**Z**		**-Y**		**-X**								**-Z**	
Position		**1**	2	**3**	4	**5**	6	**7**	8	**9**	10	11^a	11^b	12	13	14	**15**	
Consensus pattern		**D**	F	**D**	G	**D**	G	**H**	I	D	L	W	G	D	P	V	**D**	
for EF-hand calcium-			G	**N**	D	**N**		**K**	R	N	I	T	N	N	V	G		
binding domains in MltBs			Y	**S**	N			**R**	K			V	S	S	I	R		
					S			**E**					T		H	T		
																D		
																A		
																Y		
Structure																P		

variability in other EF-hand calcium-binding domains as well. Often it is a water molecule bound between the metal ion and a sidechain residue as observed in the second EF-hand domain of carp parvalbumin B [28], for example. In Slt35, there is also a water molecule at this position, but it is 3.3 Å from the ion, too far away to be a coordinating ligand. The metal ion in EF-hand domain of Slt35 is therefore missing a ligand at position 9.

Asp248 at position 12 is not ligating the ion either; its role has been taken over by the sidechain of Asp251 at position 15, which occupies a position equivalent to the calcium-binding glutamate residue at position 12 in parvalbumin B. Both residues are the third residue of the C-terminal α helix of the EF-hand domain. A superposition of the EF-hand domains of carp parvalbumin B and Slt35 shows that in Slt35 the ion-binding loop starts to deviate after position 9 and that three extra residues are inserted (Figure 3c). This results in a translation of the C-terminal α helix of the EF-hand domain (Figure 3d). This is the first time that such a variation of the EF-hand motif is observed.

A sequence comparison shows that other MltB transglycosylases also conform to the EF-hand consensus motif (Figures 2,4). The aspartate residue at position 1 and the glycine residue at position 6 are strictly conserved, whereas the –Z ligand varies from position 15 to 16 because of an insertion of one extra residue between positions 11 and 12 (Figure 4). The glycine residue at position 6 has ϕ/ψ angles that are not allowed for other amino acid residues (ϕ = 90.8°, ψ = –4.7°) and might be important for the conformation of the metal ion binding loop. At positions 3, 5, 9 and 12, serine, asparagine or aspartate residues can be present. The residue at position 10 is either leucine or isoleucine. In Slt35, the sidechain of this residue (Leu246) forms a hydrophobic cluster together with the conserved residues Ile174, Met221, Phe226 and Trp247. This indicates the conservation of the Slt35 EF-hand domain in all MltB transglycosylases.

The resemblance of the ion-binding site in Slt35 to the EF-hand calcium-binding domains suggests that a calcium ion is bound. Although the average ion ligand distance is 2.4 Å, which is typical for calcium–oxygen distances [31], we cannot rule out that a sodium ion has bound to the ion-binding site, as sodium–oxygen distances are also 2.4 Å [31]. Moreover, sodium, but not calcium, was present in the crystallisation solutions. Refinement of the metal ion as a sodium ion resulted in an atomic displacement parameter (16.0 $Å^2$) that is much closer to the average atomic displacement parameter of the ligands (15.5 $Å^2$) than when refined as a calcium ion (26.7 $Å^2$). When an Slt35 crystal was soaked in mother liquor with 1 mM $CaCl_2$, however, the sodium ion was clearly replaced by a calcium ion [32]. As the calcium ion concentration in the periplasm is in the order of 0.1–1.0 mM [33], it is probable that the naturally bound ion is a calcium ion.

Function of the calcium-binding site

In eukaryotic proteins, EF-hand calcium-binding domains can be involved in calcium sensoring, signal transduction, contraction, secretion, protein–protein recognition and cell proliferation [29,34,35]. So far only one other prokaryotic EF-hand-like domain has been described, occurring as a single domain in the periplasmic *D*-galactose-binding proteins from *E. coli* [36] and *Salmonella typhimurium* [37]. As in Slt35, this domain does not conform to the canonical EF-hand consensus sequence [29,36]; it contains two polypeptide stretches (residues 134–142 and 204–205) that are distant in the primary structure contributing to the calcium ligation [36]. The function of this domain has not been established but it might have a structural rather than regulatory role [36].

The function of the EF-hand domain in Slt35 is not clear either. As the calcium site is 20 Å from the active site (see below), a direct role in the reaction mechanism seems unlikely. Introduction of a calcium site in the human lysozyme at a position equivalent to the EF-hand calcium

Figure 5

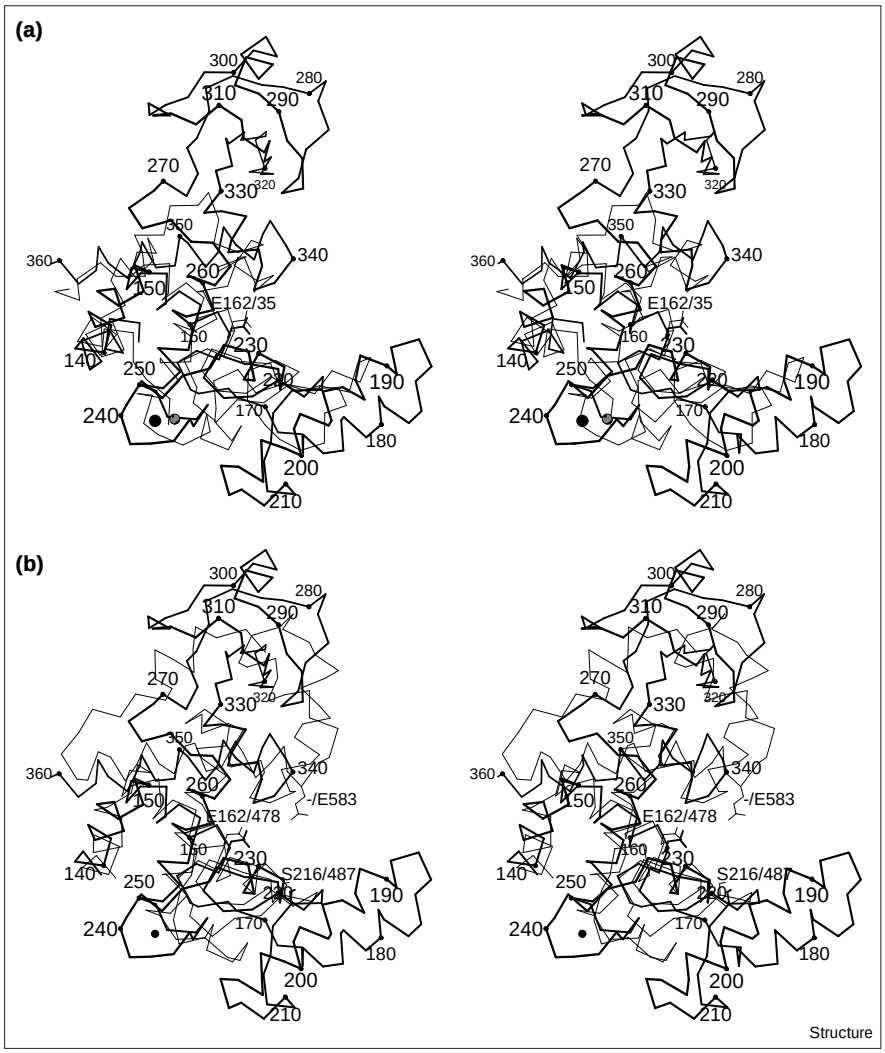

Structural comparisons with Slt35. (a) Stereoview superposition of the Cα traces of Slt35 (residues 129–361; thick black line) and human D86/92 lysozyme (residues 1–130; thin black line; PDB entry code 3lhm). The rmsd for 78 superimposed Cα atoms is 2.1 Å. The catalytic acid/base Glu162 of Slt35 and Glu35 of lysozyme are indicated. The metal ions in Slt35 and lysozyme are coloured in black and grey, respectively. (b) Stereoview superposition of the Cα traces of Slt35 (residues 137–361; thick black line) and the Slt70 catalytic domain (residues 453–618; thin black line). Glu162 and Ser216 of Slt35 and Glu478, Ser487 and Glu583 of Slt70 are indicated. The alignments were performed with the LSQ options in the program O [57]. This figure was made with the program MOLSCRIPT [64].

site in Slt35 (Figure 5a) increased the stability of the enzyme against protease digestion and thermal denaturation [38]. Such a structural function might also be possible for Slt35. Alternatively, calcium binding might be important for the correct folding of MltB in the periplasmic space. Finally, the EF-hand domain might be involved in interactions of MltB transglycosylases with other proteins such as the penicillin-binding proteins [11].

Comparison with Slt70

Despite the lack of obvious sequence similarity, the core domain of Slt35 clearly resembles the fold of the C-terminal catalytic domain of Slt70, the 70 kDa soluble lytic transglycosylase from *E. coli* [22,27]. The two domains can be superimposed with a root mean square deviation (rmsd) of 1.7 Å for 100 Cα atoms (Figure 5b). A structure-based sequence alignment shows that 23 of the 100 superimposed residues are identical (data not shown). The large excursions into the alpha and beta domains, and the absence in Slt35 of the Slt70 α helices Cα6 and Cα7 and the C-terminal tail precluded a successful sequence alignment of Slt35 and Slt70 in the past. Furthermore, Slt35 lacks the characteristic sequence motifs found in other lytic transglycosylases [7,20] also hampering a successful sequence alignment. This lack of obvious homology reflects the pronounced sequence variability and diversity in the lytic transglycosylase family.

Identification of the active site

The large groove between the alpha domain and the core domain is lined with the aromatic residues Tyr117, Phe121, Tyr191, Phe192, Phe217, Phe226, Tyr234, Tyr259, Tyr338 and Tyr344. A multiple sequence alignment of MltB transglycosylases from various species shows that the aromatic character of most of these residues is conserved (Figure 2). As aromatic residues in enzymes have often been found to interact with sugar residues in peptidoglycan, chitin and

starch [23,39,40], this suggests that the groove of Slt35 is designed to bind the peptidoglycan glycan strands and that the active site is located in this groove.

Superposition of the Slt35 core domain on the catalytic domain of Slt70 shows that Glu162 of MltB superimposes on Glu478 of Slt70 (Figure 5b). As Glu478 acts as the catalytic acid/base in Slt70 [27], this suggests that Glu162 could be the catalytic acid/base in Slt35. Indeed, a Glu162→Gln mutation results in a completely inactive enzyme (data not shown). The environment of Glu162 is largely hydrophobic stabilising the protonated state of this residue. It is surrounded by the sidechains of Ile158, Gln225, Tyr338 and Tyr344. These residues are not only conserved in Slt35 and Slt70, but also in the MltBs from other species. The Tyr344 hydroxyl group makes a strong hydrogen bond of 2.6 Å to one of the Oε atoms of Glu162. In Slt70, the equivalent Tyr587 makes a similar hydrogen bond to the acid/base catalyst Glu478.

Previously, attempts to locate the active site of MltB using the lytic transglycosylase sequence motifs of Slt70 [20,41] had suggested Glu206 as the catalytic acid/base [15]. A Glu206→Gln mutation had no effect on the activity of MltB [18]. In our structure, Glu206 is located at the surface of the alpha domain in the loop after α helix H9, distant from the putative active site (see Figure 1 for example) explaining the absence of adverse effects on the enzyme activity.

The Slt35–GlcNAc complex

To analyse whether sugars can be bound in the active site, the structure of an Slt35–GlcNAc complex was determined at 2.45 Å resolution (Table 2). The model has 201 water molecules, one sodium ion, one GlcNAc molecule and alternate sidechain conformations of Asp74, Trp145, Glu153 and Arg204. The GlcNAc sugar has been modelled in a full $^4C_1$ chair conformation (Figure 6). It is located in the active-site cleft at a distance from the catalytic Glu162, which corresponds to substrate-binding site *–2* [42]. No electron density was observed that could account for other GlcNAc molecules bound in the groove. Its O1-hydroxyl group is in a β-anomeric configuration making a water-mediated hydrogen bond to the backbone carbonyl oxygen atom of Gln225. The nitrogen atom of GlcNAc forms a hydrogen bond to the backbone carbonyl oxygen atom of Tyr338 (3.1 Å), whereas the oxygen atom of the *N*-acetyl group makes hydrogen bonds with the mainchain NH of Met227 (3.1 Å) and the Oγ of Ser230 (2.8 Å). Other hydrogen bonds are present between the C3-hydroxyl group and the Tyr259 hydroxyl group (2.8 Å), and between the C4-hydroxyl group and the Nε2 of His340 (3.1 Å). The hydroxyl group of the C6 atom has no direct contacts with protein atoms.

Comparison of the native Slt35 and Slt35–GlcNAc structures shows that a bicine buffer molecule is bound in the native Slt35 structure at a position equivalent to that of the sugar in the Slt35–GlcNAc complex (Figure 6). One of the ethylhydroxy groups of the bicine molecule mimics the position of the GlcNAc *N*-acetyl oxygen atom with hydrogen bonds to the backbone NH of Met227 (3.0 Å) and the Oγ of Ser230 (2.6 Å). The other ethylhydroxy group makes hydrogen bonds to the backbone carbonyl oxygen of Gln225 (2.7 Å) and a water molecule (3.1 Å). Furthermore, the bicine molecule has hydrophobic interactions with the aromatic rings of Phe226, Tyr259 and Tyr338 that are similar to those of the *N*-acetylmethyl group (C8) of GlcNAc.

Figure 6e shows that the mainchain atoms of Tyr338, Asn39 and His340, located above the active-site cleft, have moved 0.5–0.6 Å towards the GlcNAc sugar, to form hydrogen bonds to the N2 and O4 atoms of GlcNAc, respectively. Small active-site movements and the formation of hydrogen bonds between the *N*-acetyl group of GlcNAc in site *–2* and the protein have also been observed in the phage T4 lysozyme–murotetrapeptide complex [43], the Slt70–bulgecin complex [23] and the hen egg white lysozyme–GlcNAc complex [44].

Beside bicine, an ethylene glycol molecule has been identified in the active-site groove (Figure 6). It is bound in front of sugar-binding site –1 at the interface between the alpha and core domains about 10 Å from Glu162 and its hydroxyl groups are hydrogen bonded to the Nη1 (3.1 Å) and the Nη2 atoms (2.8 Å) of Arg188. Its carbon atoms have hydrophobic interactions with the Cε and Sδ of Met227 and the Cβ of Ala218. Arg188 and Ala218 are conserved in all MltB transglycosylases, whereas in one case there is an isoleucine residue instead of a Met227 residue (Figure 2). Modelling studies (on the basis of the T4 lysozyme–murotetrapeptide complex [45]) suggest that the ethylene glycol molecule has bound at a position where the *D*-lactyl group of a MurNAc residue in site –1 might be bound (not shown).

Peptidoglycan binding and reaction mechanism

Enzyme–substrate binding studies have shown the presence of five or six sugar-binding sites in the active-site cleft of various lysozymes [42]. The cleft of Slt35 is shorter than that in other lysozymes and seems to have only four sugar-binding sites: those at positions *–2*, –1, +1 and *+2*. Sites –3 and –4 seem to be absent because no clear sugar-binding sites are present. Preliminary modelling studies show that MurNAc residues cannot bind at the *–2* and +1 sites because of clashes of the *D*-lactyl group with Slt35 residues. Therefore, MurNAc has to bind in site –1, which explains why the enzyme is a muramidase.

In the proposed reaction mechanism of Slt70 [23], cleavage of the glycosidic bond between the C1 atom of MurNAc in site –1 and the O4 atom of GlcNAc in site +1

Figure 6

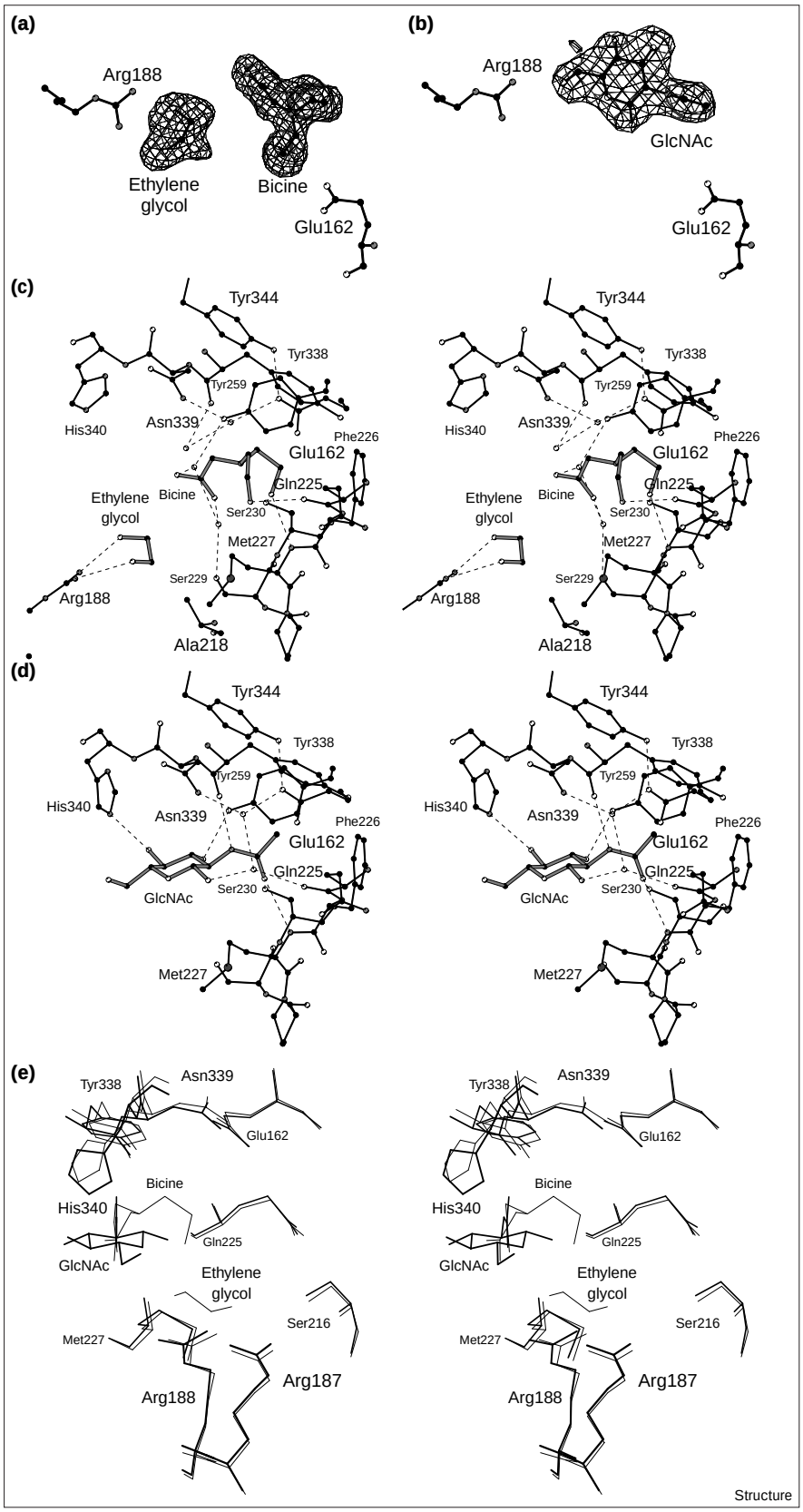

Bicine, ethylene glycol and GlcNAc in the active-site cleft of Slt35. The σ_A-weighted F_o–F_c electron density omit maps are superimposed on (a) the bicine and ethylene glycol molecules in the native Slt35 structure and (b) the GlcNAc molecule in the Slt35–GlcNAc complex. The omit maps are contoured at 3.0σ. The densities have been calculated from the final models excluding the particular molecule(s). The substrate atoms, Glu162 and Arg188 are represented in ball-and-stick representation with carbon atoms in black, nitrogen atoms in light grey, oxygen atoms in white and sulphur atoms in dark grey. (c) Stereoview of the binding interactions of bicine and ethylene glycol. Hydrogen bonds are shown as dashed lines. (d) Stereoview of the binding interactions of the GlcNAc molecule in the active site. (e) Superposition of the active sites of the native Slt35 structure (thin black line) and the Slt35–GlcNAc complex after superposition of their Cα atoms (rmsd of 0.27 Å for 312 Cα atoms).

Figure 7

Stereoview of the molecular surface of Slt35 with GlcNAc (orange) in the active site and a model for the exo-loop (residues 99–108; red). The surface is coloured according to conservation in the multiple sequence alignment of MltB transglycosylases shown in Figure 2: non-conserved residues (dark blue), similar (green), and identical (white). The surface of the catalytic acid/base Glu162 is in yellow. The residues of the exo-loop, which are currently missing in the X-ray structure, have been modelled in the program O in a region of low electron density and refined with X-PLOR.

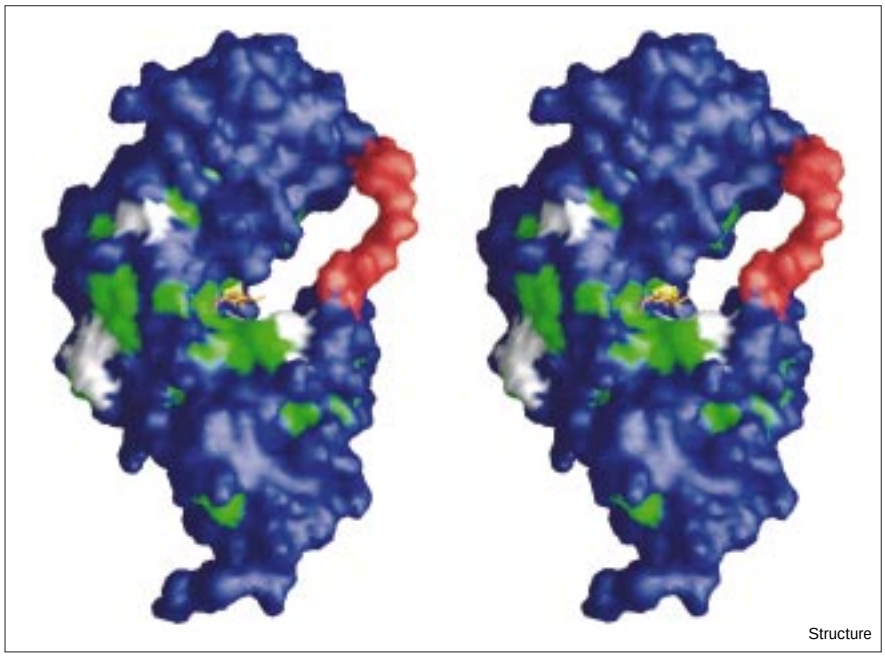

is assumed to result in the formation of an oxo-carbonium ion-like transition state on the –1 MurNAc residue. This reaction intermediate state could be stabilised by the 2-acetamido group of the –1 MurNAc residue. In Slt70, residues Ser487 and Glu583 contribute to the correct orientation and stabilisation of the 2-acetamido group by hydrogen bonding to the 2-acetamido oxygen and nitrogen atoms [23]. Such a substrate-assisted stabilisation has also been described for the plant chitinase hevamine [46] and the *Serratia marcescens* chitobiase [47], in which carboxylate and hydroxyl groups also help to orient the 2-acetamido group in a similar manner. Residue Ser216 of Slt35 superimposes on Ser487 of Slt70, but surprisingly there is no residue in a position equivalent to that of Glu583 in Slt70. Whether this difference is of functional importance for the catalytic mechanism or regulation of the activity requires further investigation.

Exo-muramidase activity

Slt35 is an exo-muramidase that cleaves 1,6-anhydromuropeptides from the non-reducing GlcNAc end of peptidoglycan strands processing towards the 1,6-anhydromuramate end [48]. Slt70 is also an exo-muramidase [48] and it has been proposed that the doughnut-shaped N-terminal domain of Slt70 is responsible for its activity as an exo-enzyme [22]. Slt35 lacks such a doughnut-shaped domain, but instead the disordered residues 99–108 might partly cover the active site (Figure 7) and thus might prevent endo-activity of the enzyme. Additionally, this exo-loop might cause steric hindrance with the peptide crossbridges in the peptidoglycan and this might restrict the activity of Slt35 to peptidoglycan with either no degree or a low degree of cross-linking.

Biological implications

An intact cell wall is of vital importance for the survival of bacteria. Compounds that interfere with the strictly regulated activity of the enzymes involved in the synthesis and degradation of the cell wall peptidoglycan have been found to be effective antibiotics. Whereas penicillin and related β-lactam antibiotics inactivate the enzymes that make and break the peptide bonds in the peptidoglycan, only a few inhibitors are known for the enzymes that act on the glycan strands of peptidoglycan.

Lytic transglycosylases catalyse the cleavage of the β-1,4-glycosidic bond between an *N*-acetylmuramic acid (MurNAc) residue and *N*-acetylglucosamine (GlcNAc) residue in peptidoglycan with concomitant formation of a 1,6-anhydrobond between the O6 and C1 atoms in the MurNAc residue. In total, six different lytic transglycosylases (Slt70, MltA–D and EmtA) have been characterized in *Escherichia coli*; they differ in size, sequence, activity, specificity and location. As inhibition of certain lytic transglycosylases strongly enhances the effect of some β-lactam antibiotics, the development of lytic transglycosylase inhibitors is considered to be a valuable approach to increase the array of effective antibacterial compounds.

The present study describes the crystal structure of the *E. coli* lytic transglycosylase Slt35, a soluble 36 kDa form of the slightly larger outer membrane bound

lipoprotein MltB (40 kDa). Although Slt35 has no obvious sequence similarity to Slt70, the only other structurally characterised lytic transglycosylase, its catalytic domain shows a surprising similarity to that of Slt70. The active site is very similar as well, with the exception of one carboxylic residue which is absent in Slt35, but which in Slt70 probably interacts with the 2-acetamido moiety of the MurNAc residue during catalysis. Nevertheless, the similarity of the active sites of Slt35 and Slt70 suggests that it might be possible to develop new antibacterial inhibitors that target several lytic transglycosylases at once.

Materials and methods

Crystallisation

For the expression and crystallisation of Slt35, an active 36 kDa soluble fragment was constructed, which starts at residue 42 with two additional residues (Met40 and Val41) at the N terminus [15]. Slt35 crystallises in the presence of 0.1 M bicine-NaOH buffer (pH 7.8–8.5) and 0–6% polyethylene glycol 20,000 (PEG20K) in the primitive orthorhombic space group $P2_12_12_1$ with cell dimensions of a = 58.3, b = 67.9 and c = 98.9 Å [49]. The value of the Matthews coefficient, V_m [50], is 2.72 Å^3/Da for one molecule per asymmetric unit. Assuming a partial specific volume for globular proteins of 0.74 cm^3/g, the solvent content of the crystals is about 55%. Crystals were stored in a stabilising solution containing 100 mM bicine-NaOH buffer (pH 8.0–8.5), 1% isopropanol and 5–10% PEG20K.

GlcNAc soaking experiment

In the native Slt35 structure, a bicine molecule (*N*, *N*-bis[2-hydroxyethyl]-glycine) and an ethylene glycol molecule, probably originating from the PEG20K solution, were observed in the active site. To avoid any interference with the binding of *N*-acetylglucosamine (GlcNAc), a 25% (w/v) PEG20K stock solution was dialysed against pure water for 24 h using a membrane with a 6–10 kDa cut-off. The concentration of the PEG20K was determined with a GPR 11–37 Refractometer (Index Instruments). An Slt35 crystal was washed in a solution of 50 mM Tris-HCl buffer (pH 8.0) and 2% of dialysed PEG20K and this was repeated four times in 30 min. Subsequently, the crystal was soaked for 18 min in a solution of 50 mM Tris-HCl buffer (pH 8.0), and 2% of dialysed PEG20K saturated with GlcNAc (Sigma).

Data collection and processing

For diffraction experiments, crystals were flash frozen at 120K in a stream of evaporating nitrogen after having been soaked for 1 min in a cryo-protectant consisting of 25–50% glycerol added to the stabilising or soaking solution. Data to 1.7 Å resolution were collected from a native Slt35 crystal at the A1 station at CHESS (Cornell High Energy Synchrotron Source) in Ithaca (USA), using a wavelength of 0.920 Å and a CCD camera as detector. Slt35–GlcNAc diffraction data were collected on a DIP 2030H image plate (MacScience) using Cu Kα radiation from a Nonius FR591 rotating-anode generator with Franks' mirrors. Data were processed with DENZO and SCALEPACK [51]. Intensities were converted to structure-factor amplitudes with programs from the Groningen BIOMOL software package.

In the course of an extensive heavy-atom derivative search, diffraction data were collected on a FAST area detector (Enraf-Nonius, Delft, The Netherlands) using Cu Kα radiation from an Enraf Nonius FR571 rotating-anode generator with a graphite monochromator. Data reduction was performed with MADNES [52], XDS [53] and BIOMOL programs. Data for a mercury derivative (Hg-III) were measured at beamline BW7A of the EMBL Outstation at DESY, Hamburg (Germany), at a wavelength of 0.970 Å with a MAR Research (Hamburg) imaging plate as detector. These data were also processed with DENZO and SCALEPACK. Data collection statistics can be found in Table 1.

Phasing

The structure of Slt35 was solved by the multiple isomorphous replacement method with inclusion of anomalous scattering differences (MIRAS) (Table 1). Heavy-atom parameters were scaled and refined at 2.7 Å resolution with PHASES [54]. The MIRAS phases were subsequently extended to 2.5 Å resolution using the program DM [55] with solvent flattening and histogram matching. Next the recently developed wARP procedure [56] was used to improve and extend the phases to 2.0 Å resolution, which resulted in a map that was readily interpretable. Later, it appeared that the 2.5 Å DM phases could be readily extended to even 1.7 Å resolution using wARP as described in detail elsewhere [49].

Model building and refinement

Model building was performed with the interactive graphics program O [57] on Silicon Graphics workstations. The quality of the wARP map allowed us to take complete advantage of the model building procedures and especially the real-space refinement capabilities included in the O package. The model from O was refined at 1.7 Å resolution in several cycles of simulated annealing (3000–300K), Powell energy minimisation, overall and individual B-factor refinement with the program X-PLOR version 3.843 [58] and manual rebuilding. For a test set, 10% of randomly selected reflections were set aside [59]. At the end of the refinement, low resolution diffraction data to 20 Å were included and a bulk-solvent correction was applied. The application of resolution-dependent and $1/\sigma^2$ weighting schemes resulted in lower R_{free} values and smaller differences between R_{work} and R_{free}.

The native Slt35 model was used as a starting model to refine the Slt35–GlcNAc complex. The same reflections were selected for the test set as were used in the refinement of the native data set (10% of reflections) [59]. After rigid-body refinement (3.5–8.0 Å resolution), the model was refined in several cycles of Powell energy minimisation, occupancy refinement of alternate sidechain conformations, overall and individual B-factor refinement with the program X-PLOR version 3.843 [58]. Solvent molecules and GlcNAc were added to complete the model. The force constants and parameters used for the sugar were those described by Weis *et al.* [60], and as implemented in the X-PLOR geometry files. Low resolution diffraction data to 20 Å, a bulk-solvent correction, an anisotropic B-factor scaling and resolution-dependent and $1/\sigma^2$ weighting schemes were included.

The last refinement cycle of both structures was repeated with all data including the test set. The final refinement statistics for both structures are summarised in Table 2. Stereochemistry was inspected with the programs PROCHECK [61] and WHAT CHECK [62]. Surface calculations were performed with ASC [63] using a probe radius of 1.4 Å.

Mutagenesis

The codon for Glu162 was exchanged for one coding for a glutamine residue, using the QuickChange mutagenesis system (Stratagene, La Jolla, CA). Peptidoglycan hydrolase activity of the expressed mutant protein was determined using zymogram analysis, and by measuring the solubilization of radiolabelled peptidoglycan following a published procedure [15].

Accession numbers

Atomic coordinates have been deposited with the Protein Data Bank under the accession codes 1QUS for the native structure and 1QUT for the Slt35 complex.

Acknowledgements

We thank Anastassis Perrakis (EMBL Outstation, Grenoble) and Victor Lamzin (EMBL Outstation, Hamburg) for a stimulating collaboration on wARP. Andy-Mark Thunnissen, Daniel Thiel and Marian Szebenyi are acknowledged for their help during data collection at CHESS. We thank the European Union for support of the work at EMBL Hamburg through the HCMP Access to Large Installations Project, Contract Number CHGE-CT93-0040. The investigations were supported by the Netherlands Foundation for Chemical Research (SON) with financial aid from the Netherlands Organization for Scientific Research (NWO).

References

1. Kock, A.L. (1988). Biophysics of bacterial walls viewed as stress-bearing fabric. *Microbiol. Rev.* 52, 337-353.
2. Höltje, J.V. (1998). Growth of the stress-bearing and shape-maintaining murein sacculus of *Escherichia coli*. *Microbiol. Mol. Biol. Rev.* 62, 181-203.
3. Park, J.T. & Strominger, J.L. (1957). Mode of action of penicillin. Biochemical basis for the action of penicillin and for its selective toxicity. *Science* 125, 99-101.
4. Gold, H.S. & Moellering Jr., R.C. (1996). Antimicrobial-drug resistance. *N. Engl. J. Med.* 335, 1445-1453.
5. Höltje, J.V., Mirelman, D., Sharon, N. & Schwarz, U. (1975). Novel type of murein transglycosylase in *Escherichia coli*. *J. Bacteriol.* 124, 1067-1076.
6. Höltje, J.V. (1995). From growth to autolysis: the murein hydrolases in *Escherichia coli*. *Arch. Microbiol.* 164, 243-254.
7. Dijkstra, A.J. & Keck, W. (1996). Peptidoglycan as a barrier to transenvelope transport. *J. Bacteriol.* 178, 5555-5562.
8. Höltje, J.V. & Tuomanen, E.I. (1991). The murein hydrolases of *Escherichia coli*: properties, functions and impact on the course of infections *in vivo*. *J. Gen. Microbiol.* 137, 441-454.
9. Kitano, K., Tuomanen, E. & Tomasz, A. (1986). Transglycosylase and endopeptidase participate in the degradation of murein during autolysis of *Escherichia coli*. *J. Bacteriol.* 167, 759-765.
10. Höltje, J.V. (1996). Molecular interplay of murein synthases and murein hydrolases in *Escherichia coli*. *Microb. Drug Resist.* 2, 99-103.
11. von Rechenberg, M., Ursinus, A. & Höltje, J.V. (1996). Affinity chromatography as a means to study multienzyme complexes involved in murein synthesis. *Microb. Drug Resist.* 2, 155-157.
12. Ursinus, A. & Höltje, J.V. (1994). Purification and properties of a membrane-bound lytic transglycosylase from *Escherichia coli*. *J. Bacteriol.* 176, 338-343.
13. Lommatzsch, J., Templin, M.F., Kraft, A.R., Vollmer, W. & Höltje, J.-V. (1997). Outer membrane localization of murein hydrolases: MltA, a third lipoprotein lytic transglycosylase in *Escherichia coli*. *J. Bacteriol.* 179, 5465-5470.
14. Engel, H., Smink, A.J., van Wijngaarden, L. & Keck, W. (1992). Murein-metabolizing enzymes from *Escherichia coli*: existence of a second lytic transglycosylase. *J. Bacteriol.* 174, 6394-6403.
15. Dijkstra, A.J., Hermann, F. & Keck, W. (1995). Cloning and controlled overexpression of the gene encoding the 35 kDa soluble lytic transglycosylase from *Escherichia coli*. *FEBS Lett.* 366, 115-118.
16. Ehlert, K., Höltje, J.V. & Templin, M.F. (1995). Cloning and expression of a murein hydrolase lipoprotein from *Escherichia coli*. *Mol. Microbiol.* 16, 761-768.
17. Dijkstra, A.J. & Keck, W. (1996). Identification of new members of the lytic transglycosylase family in *Haemophilus influenzae* and *Escherichia coli*. *Microb. Drug Resist.* 2, 141-145.
18. Dijkstra, A.J. (1997). *The soluble lytic transglycosylase family of Escherichia coli.* In vitro *activity versus* in vivo *function.* PhD Thesis, University of Groningen.
19. Kraft, A.R., Templin, M.F. & Höltje, J.V. (1998). Membrane-bound lytic endoglycosylase in *Escherichia coli*. *J. Bacteriol.* 180, 3441-3447.
20. Koonin, E.V. & Rudd, K.E. (1994). A conserved domain in putative bacterial and bacteriophage transglycosylases. *TIBS* 19, 106-107.
21. Bayer, M., Eferl, R., Zellnig, G., Teferle, K., Dijkstra, A., Koraimann, G. & Hoenauer, G. (1995). Gene 19 of plasmid R1 is required for both efficient conjugative DNA transfer and bacteriophage R17 infection. *J. Bacteriol.* 177, 4279-4288.
22. Thunnissen, A.M.W.H., Dijkstra, A.J., Kalk, K.H., Rozeboom, H.J., Engel, H., Keck, W. & Dijkstra, B.W. (1994). Doughnut-shaped structure of a bacterial muramidase revealed by X-ray crystallography. *Nature* 367, 750-753.
23. Thunnissen, A.M.W.H., Rozeboom, H.J., Kalk, K.H. & Dijkstra, B.W. (1995). Structure of the 70-kDa soluble lytic transglycosylase complexed with bulgecin A. Implications for the enzymatic mechanism. *Biochemistry* 34, 12729-12737.
24. Templin, M.F., Edwards, D.H. & Höltje, J.V. (1992). A murein hydrolase is the specific target of bulgecin in *Escherichia coli*. *J. Biol. Chem.* 267, 20039-20043.
25. Holm, L. & Sander, C. (1994). The FSSP database for structurally aligned protein fold families. *Nucleic Acids Res.* 22, 3600-3609.
26. Weaver, L.H., Grutter, M.G. & Matthews, B.W. (1995). The refined structures of goose lysozyme and its complex with a bound trisaccharide show that the "goose-type" lysozymes lack a catalytic aspartate residue. *J. Mol. Biol.* 245, 54-68.
27. Thunnissen, A.M.W.H., Isaacs, N.W. & Dijkstra, B.W. (1995). The catalytic domain of a bacterial lytic transglycosylase defines a novel class of lysozymes. *Proteins: Struct. Funct. Genet.* 22, 245-258.
28. Swain, A.L., Kretsinger, R.H. & Amma, E.L. (1989). Restrained least squares refinement of native (calcium) and cadmium-substituted carp parvalbumin using X-ray crystallographic data at 1.6-Å resolution. *J. Biol. Chem.* 264, 16620-16628.
29. Kretsinger, R. (1997). EF-hands embrace. *Nat. Struct. Biol.* 4, 514-516.
30. Babu, Y.S., C.E., B. & Cook, W.J. (1988). Structure of calmodulin at 2.2 Å resolution. *J. Mol. Biol.* 204, 191-204.
31. Shannon, R.D. (1976). Revised effective ionic radii and systematic studies of interatomic distances in halides and chalcogenids. *Acta Crystallogr. A* 32, 751-767.
32. van Asselt, E.J. & Dijkstra, B.W. (1999). Binding of calcium in the EF-hand of *Escherichia coli* lytic transglycosylase Slt35 is important for stability. *FEBS Lett.* In press.
33. Norris, V., *et al.* & Norman, R.I. (1996). Calcium signalling in bacteria. *J. Bacteriol.* 178, 3677-3682.
34. Nakayama, S. & Kretsinger, R.H. (1994). Evolution of the EF-hand family of proteins. *Annu. Rev. Biophys. Biomol. Struct.* 23, 473-507.
35. Ames, J.B., Ishima, R., Tanaka, T., Gordon, J.I., Stryer, L. & Ikura, M. (1997). Molecular mechanics of calcium-myristoyl switches. *Nature* 389, 198-202.
36. Vyas, N.K., Vyas, M.N. & Quiocho, F.A. (1987). A novel calcium binding site in the galactose-binding protein of bacterial transport and chemotaxis. *Nature* 327, 635-638.
37. Zou, J.Y., Flocco, M.M. & Mowbray, S.L. (1993). The 1.7 Å refined X-ray structure of the periplasmic glucose/galactose receptor from *Salmonella typhimurium*. *J. Mol. Biol.* 233, 739-752.
38. Kuroki, R., Taniyame, Y., Seko, C., Nakamura, H., Kikuchi, M. & Ikehara, M. (1989). Design and creation of a Ca^{2+} binding site in human lysozyme to enhance structural stability. *Proc. Natl Acad. Sci USA* 86, 6903-6907.
39. Terwisscha van Scheltinga, A.C., Kalk, K.H., Beintema, J.J. & Dijkstra, B.W. (1994). Crystal structures of hevamine, a plant defence protein with chitinase and lysozyme activity, and its complex with an inhibitor. *Structure* 2, 1181-1189.
40. Strokopytov, B., Knegtel, R.M.A., Penninga, D., Rozeboom, H.J., Kalk, K.H., Dijkhuizen, L. & Dijkstra, B.W. (1996). Structure of cyclodextrin glycosyltransferase complexed with a maltononaose inhibitor at 2.6 Å resolution. Implications for product specificity. *Biochemistry* 35, 4241-4249.
41. Dijkstra, B.W. & Thunnissen, A.M. (1994). 'Holy' proteins. II: The soluble lytic transglycosylase. *Curr. Opin. Struct. Biol.* 4, 810-813.
42. White, A. & Rose, D.R. (1997). Mechanism of catalysis by β-glycosyl hydrolases. *Curr. Opin. Struct. Biol.* 7, 645-651.
43. Kuroki, R., Weaver, L.H. & Matthews, B.W. (1993). A covalent enzyme substrate intermediate with saccharide distortion in a mutant T4 lysozyme. *Science* 262, 2030-2033.
44. Kurachi, K., Sieker, L.C. & Jensen, L.H. (1976). Structures of triclinic mono- and di-N-acetylglucosamine: lysozyme-complexes – a crystallographic study. *J. Mol. Biol.* 101, 11-24.
45. Kuroki, R., Weaver, L.H. & Matthews, B.W. (1995). Structure-based design of a lysozyme with altered catalytic activity. *Nat. Struct. Biol* 2, 1007-1011.
46. Terwisscha van Scheltinga, A.C., Armand, S., Kalk, K.H., Isogai, A., Henrissat, B. & Dijkstra, B.W. (1995). Stereochemistry of chitin hydrolysis by a plant chitinase/lysozyme and X-ray structure of a complex with allosamidin: evidence for substrate assisted catalysis. *Biochemistry* 34, 15619-15623.
47. Tews, I., Terwisscha van Scheltinga, A.C., Perrakis, A., Wilson, K.S. & Dijkstra, B.W. (1997). Substrate-assisted catalysis unifies two families of chitinolytic enzymes. *J. Am. Chem. Soc.* 119, 7954-7959.
48. Romeis, T., Vollmer, W. & Höltje, J.V. (1993). Characterization of three different lytic transglycosylases in *Escherichia coli*. *FEMS Microbiol. Lett.* 111, 141-146.
49. van Asselt, E.J., Perrakis, A., Kalk, K.H., Lamzin, V.S. & Dijkstra, B.W. (1998). Accelerated X-ray structure elucidation of a 36 kDa muramidase/transglycosylase using wARP. *Acta Crystallogr.* D 54, 58-73.
50. Matthews, B.W. (1968). Solvent content of protein crystals. *J. Mol. Biol.* 33, 491-497.
51. Otwinowski, Z. & Minor, W. (1997). Processing of X-ray diffraction data collection in oscillation mode. *Methods Enzymol.* 276, 307-326.
52. Messerschmidt, A. & Pfugrath, J.W. (1987). Crystal orientation and X-ray pattern prediction routines for area detector diffractometer systems in macromolecular crystallography. *J. Appl. Cryst.* 20, 306-315.

53. Kabsch, W. (1988). Evaluation of single-crystal X-ray diffraction data from a position-sensitive detector. *J. Appl. Cryst.* 21, 916-924.
54. Furey, W. & Swaminathan, S. (1997). PHASES-95; a program package for the processing and analyzing diffraction data from
55. Cowtan, K.D. & Main, P. (1993) Improvement of macro-molecular electron-density maps by the simultaneous application of real and reciprocal space constraints. *Acta Crystallogr.* D 49, 148-157.
56. Perrakis, A., Sixma, T.K., Wilson, K.S. & Lamzin, V.S. (1997). wARP: Improvement and extension of crystallographic phases by weighted averaging of multiple-refined dummy atomic models. *Acta Crystallogr.* D 53, 448-455.
57. Jones, T.A., Zou, J.Y., Cowan, S.W. & Kjeldgaard, M. (1991). Improved methods for building protein models in electron density maps and the location of the errors in these models. *Acta Crystallogr. A* 47, 110-119.
58. Brünger, A.T. (1992). *X-PLOR. A system for crystallography and NMR*, Yale University, New Heaven, CT, USA.
59. Brünger, A.T. (1992). Free R value: a novel statistical quantity for assessing the accuracy of crystal structures. *Nature* 355, 472-475.
60. Weis, W.I., Brünger, A.T., Skehel, J.J. & Wiley, D.C. (1990). Refinement of the influenza virus hemagglutinin by simulated annealing. *J. Mol. Biol.* 212, 737-761.
61. Laskowski, R.A., MacArthur, M.W., Moss, D.S. & Thornton, J.M. (1993). PROCHECK: a program to check the stereochemical quality of protein structures. *J. Appl. Cryst.* 26, 283-291.
62. Hooft, R.W.W., Vriend, G., Sander, C. & Abola, E.E. (1996). Errors in protein structures. *Nature* 381, 272.
63. Eisenhaber, F. & Argos, P. (1993). Improved strategy in analytic surface calculation for molecular systems: handling of singularities and computational efficiency. *J. Comp. Chem.* 14, 1272-1280.
64. Kraulis, P.J. (1991). MOLSCRIPT: a program to produce both detailed and schematic plots of protein structures. *J. Appl. Cryst.* 24, 946-950.
65. Thompson, J.D., Higgins, D.G. & Gibson, T.J. (1994). CLUSTAL W: Improving the sensitivity of progressive multiple sequence alignment through sequence weighting, positions-specific gap penalties and weight matrix choice. *Nucleic Acids Res.* 22, 4673-4680.
66. Barton, G.J. (1993). ALSCRIPT a tool to format multiple sequence alignments. *Protein Eng.* 6, 37-40.
67. Altschul, S.F., Madden, T.L., Schiffer, A.A., Zhang, J., Zhang, Z., Miller, W. & Lipman, D.J. (1997). Gapped BLAST and PHI-BLAST: a new generation of protein database search programs. *Nucleic Acids Res.* 25, 3389-3402.
68. Engh, R.A. & Huber, R. (1991). Accurate bond and angle parameters for X-ray protein structure refinement. *Acta Crystallogr. A* 47, 392-400.